entropy

MDPI

Article

Entropy-Based Method for Evaluating Contact Strain-Energy Distribution for Assembly Accuracy Prediction

Yan Fang, Xin Jin *, Chencan Huang and Zhijing Zhang *

School of Mechanical Engineering, Beijing Institute of Technology, Beijing 100081, China; fangyan@bit.edu.cn (Y.F.); hccbit@163.com (C.H.)

* Correspondence: jinxinbit@163.com (X.J.); zhangzhijing_mmt@hotmail.com (Z.Z.); Tel.: +86-10-689-1846 (X.J.); +86-10-689-4308 (Z.Z.)

Academic Editor: Dawn E. Holmes

Received: 6 December 2016; Accepted: 19 January 2017; Published: 24 January 2017

Abstract: Assembly accuracy significantly affects the performance of precision mechanical systems. In this study, an entropy-based evaluation method for contact strain-energy distribution is proposed to predict the assembly accuracy. Strain energy is utilized to characterize the effects of the combination of form errors and contact deformations on the formation of assembly errors. To obtain the strain energy, the contact state is analyzed by applying the finite element method (FEM) on 3D, solid models of real parts containing form errors. Entropy is employed for evaluating the uniformity of the contact strain-energy distribution. An evaluation model, in which the uniformity of the contact strain-energy distribution is evaluated in three levels based on entropy, is developed to predict the assembly accuracy, and a comprehensive index is proposed. The assembly experiments for five sets of two rotating parts are conducted. Moreover, the coaxiality between the surfaces of two parts with assembly accuracy requirements is selected as the verification index to verify the effectiveness of the evaluation method. The results are in good agreement with the verification index, indicating that the method presented in this study is reliable and effective in predicting the assembly accuracy.

Keywords: evaluation; entropy; assembly accuracy; contact strain energy

1. Introduction

Current developments in the field of precision mechanical systems, such as machining, measurement, and instrumentation, widely focus on precision assembly. Assembly accuracy significantly affects the performance of precision mechanical systems. To improve the accuracy of the assembly, it is essential to develop precision assembly. Hence, the increasing demand for the development of precision assembly puts a greater emphasis on achieving a better understanding of the formation of assembly errors and its final effect on the assembly accuracy. It is also an urgent problem to find a quantitative evaluation method able to reveal the degree of influence of these assembly errors on the final assembly accuracy.

The factors causing assembly errors are complex, including materials, assembly forces, assembly clearance, fixture error, and so on [1–4]. It is well understood that the geometry of manufactured surfaces deviates from the ideal design. For precision assembly, the geometrical defect in parts is an unavoidable basic factor, which causes assembly error. The geometric variations affect the location and orientation of mating parts, which significantly influence the final assembly accuracy. Generally, tolerance is used to characterize the geometric variation in the surfaces of parts, and current models analyzing the assembly variation are based on the geometric tolerances of parts [5–8]. In addition, tolerance is also used to roughly estimate the accuracy of assembly. The tolerance-based variation

analysis can provide the range of assembly variation, namely the upper and lower limits of assembly variation. However, for precision assembly, this type of variation analysis method does not reflect the actual assembly error caused by the defects in the parts and is difficult to be used to predict the assembly accuracy. Figure 1 shows four parts with identical tolerances (the flatness), but with different defective features. In accordance with the tolerance-based variation analysis method, the assembly error and the final assembly accuracy for these parts would be the same, but in fact they produce completely different assembly errors and lead to a completely different final assembly accuracy. When part P_2, having an ideal surface, mates with part P_1, the assembly errors for Cases (c) and (d) are consistent with the result of the tolerance-based variation analysis. However, in Cases (a) and (b), the assembly errors are considerable and the assembly accuracy is poor, indicating significant inconsistency with the result of the tolerance-based variation analysis, as shown in Figure 2.

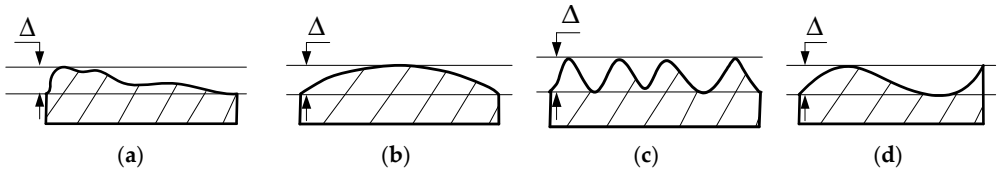

Figure 1. Four types of surface features in part P_1. (**a**) Case a; (**b**) Case b; (**c**) Case c; (**d**) Case d.

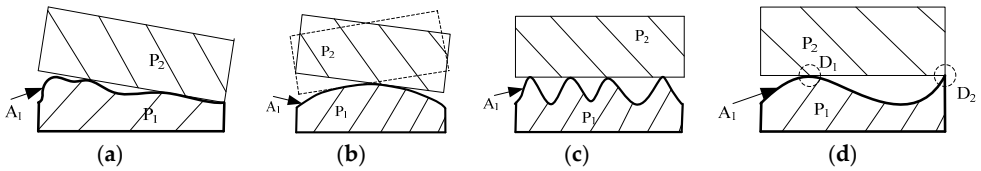

Figure 2. Location and orientation of the mating in part P_2. (**a**) Case a; (**b**) Case b; (**c**) Case c; (**d**) Case d.

To explain assembly errors more accurately, researchers established variation-analysis models by considering form errors. Pierce and Rosen [9] constructed a tolerance-analysis model with form errors by creating 3D solid parts with non-uniform rational basis spline (NURBS) surfaces. Samper et al. [10] analyzed the assembly process using a method for solving the 3D assemblies of a pair of surfaces having form errors using static equilibrium solution. Grandjeana et al. [11] proposed a method to analyze the influence of form errors on a rotating plane assembly by synthetizing the surfaces of parts, which have different values and types of form errors and position defects. Zuo et al. [12] analyzed the variation propagation in assembly processes of a precision mechanical system and developed a variation-propagation model considering the form error of mating surfaces. Armillotta et al. [13] proposed a criterion to estimate the effects of form errors on the inclusion of mating datum planes in a tolerance chain.

The aforementioned studies assume that the manufactured parts are rigid, without considering the deformation that may occur during the assembly process. However, in actual assembly processes, assembly forces can deform the contact surfaces of an assembly, thereby changing the location and orientation of the mating parts. Such variations in location and orientation can be regarded as additional assembly errors, which will significantly affect the assembly accuracy. It can be seen from Figure 2 that, if the part is considered rigid, i.e., only the effects of form errors are considered, the assembly errors for Groups (c) and (d) are still consistent with the prediction results of tolerance-based variation. However, based on the assembly force, only two points are in contact in the assembly of Group (d); the deformation of point D_2 is greater than that of point D_1, which will change the location and orientation of the mating part P_2, causing assembly error. In contrast, Group (c) has more contact points, and the deformations at the contact points are relatively consistent; hence, the assembly error is relatively small. Considering the effect of deformation, researchers have discussed the assembly-error analysis and integrated the elastic deformation and displacement of

the part. Samper et al. [14] presented four models wherein tolerance was considered in the elastic deformation mechanisms. Liu and Hu [15] developed mechanistic-variation simulation models for deformable sheet-metal parts with complex two or three-dimensional free form surfaces using the finite element method (FEM). Liu and Qiao [16] proposed a method of calculating assembly error due to part deformation. Ting et al. [17] established a deviation-calculation model based on the Jacobian-Torsor model, considering both manufacturing and deformation errors.

The aforementioned studies merely focused on the factor of form or deformation errors in assembly error analysis. However, the influence of both form and deformation errors on the formation of assembly error was not addressed. In fact, under assembly forces, form errors may cause a large local contact deformation, resulting in assembly error. Hence, the assembly error is a result of the combination of form errors and contact deformations. Such an assembly error due to the combination of form errors and contact deformations will eventually be stored in the form of strain energy on the contact surface of mating parts. Therefore, the strain energy can characterize the effects of the combination of form errors and contact deformations on the formation of assembly errors. Moreover, Figure 2 shows that, when the assembly accuracy is relatively better, as in Group (c), the effect of form errors and contact deformations on the contact surface A_1 is relatively uniform, i.e., the strain-energy distribution on the contact surface is relatively uniform. In other words, the uniformity of strain-energy distribution can indicate the accuracy of assembly formation. On the other hand, a quantitative method that can evaluate the influence of these assembly errors on the final assembly accuracy has not been addressed. Therefore, in this study, strain energy is employed to characterize the effects of the combination of form errors and contact deformations on the formation of assembly errors. In addition, an evaluation model of strain-energy distribution based on entropy is established as a quantitative method for evaluating the influence of the combination of form errors and contact deformations on the final assembly accuracy, and it can be used to predict assembly accuracy.

2. Evaluation Model

2.1. Definitions

To simplify the following discussion, some basic concepts are defined as follows, as shown in Figure 3.

1. Real machined plane with form error is abbreviated as PFE, which is an actual surface.
2. Part surface layer is abbreviated as PSL, which is the main layer influenced by the assembly force. In addition, PSL is the main occurrence zone of the contact stress and contact deformation.
3. Convex hull interface is abbreviated as CHI, which is the lower limit plane for convex hulls. The portions above this plane are regarded as components for convex hulls, which will bear assembly forces and produce high strain energy in assembly.

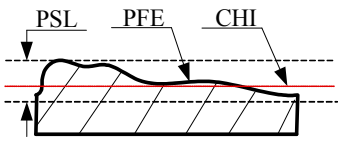

Figure 3. Schematic of defined parameters.

2.2. Evaluation Method for Contact Strain-Energy Distribution

In this study, strain energy [18] is a potential energy expressed in terms of internal deformation variables. Therefore, strain energy is employed to characterize the combination effect of form errors and contact deformations on the formation of assembly error. As strain-energy distribution can indicate assembly accuracy, we evaluate the uniformity of the strain-energy distribution to predict the assembly accuracy.

Entropy has been widely employed in control theory, image reconstruction, pattern recognition, probability theory, number theory, astrophysics, biology, and medicine [19–27]. Information entropy has a more general definition than thermodynamic entropy. In information theory, if there is a discrete random variable X with possible values, $\{x_1, \ldots, x_n\}$, and probability mass function, $P(X)$, then the entropy H of X is defined as

$$H(X) = E \log_r \left(\frac{1}{p_i} \right) = -\sum_{i=1}^{n} p_i \log_r p_i \tag{1}$$

In terms of an event, x_i, it has a probability, p_i, i.e., $p_i = P(X = x_i)$; r is the base of the logarithm, which usually takes $r = 2$ [28–33] (In this study, we take $r = 2$). The entropy $H(X)$ possesses a maximum property, which implies that the measure will be maximal if all the outcomes are equally likely. Hence, maximum entropy can be written as

$$H_{\max} = -\sum_{i=1}^{n} \frac{1}{i} \log_2 \frac{1}{i} = \log_2 n \tag{2}$$

From the maximum property of entropy, it can be found that a more disorderly system indicates that the probabilities of all possible values of the random variable are closer to each other, thereby resulting in higher entropy. Therefore, entropy can be used to evaluate probability uniformity of the possible values of a random variable. The evaluation result of the distributed uniformity of the contact strain energy is in line with the characteristics of entropy. The magnitude of strain energy is related to the volume of material selected for calculation, thus, to exclude the effect of volume, a unit volume of the strain energy is employed as the probability of the random variable, i.e., the strain-energy density. For an isotropic, linear, and elastic body, the strain-energy density w can be written as

$$w = \int_0^{\varepsilon_{ij}} \sigma_{ij} d\varepsilon_{ij} = \frac{1}{2} \sigma_{ij} \varepsilon_{ij} \tag{3}$$

where $\sigma_{ij} (i, j = x, y, z)$ and $\varepsilon_{ij} (i, j = x, y, z)$ are the components of stress and strain, respectively; x, y, and z are the directions of the three axes.

The real PSL is continuous in physical space, but when we divide the PSL into a number of virtual units, they can be considered as a system. The strain-energy densities of each unit are calculated as the probabilities of all possible values of a random variable. We denote the strain energy of each unit as $w_1, w_2, \ldots, w_m$, where m is the number of units. Considering the non-negativity and completeness of the probability, we normalize w_i as follows:

$$w_i' = \frac{w_i}{\sum_{i}^{m} w_i}, \tag{4}$$

where w_i is the strain energy density of the ith unit, and w_i' is the normalized strain-energy density of the ith unit. The entropy of the strain-energy density is defined as follows:

$$H = -\sum_{i=1}^{m} w_i' \log_2 w_i' \tag{5}$$

The corresponding maximum entropy can be expressed as

$$H_{\max} = \log_2 m \tag{6}$$

The normalized entropy can be expressed as

$$H_s = \frac{H}{H_{\max}} \tag{7}$$

As the normalized entropy increases, the strain-energy distribution becomes uniform.

Note: In the following sections, the entropies are calculated using the normalized strain-energy density, and a description thereof will not be repeated.

2.3. Evaluation Model of Contact Strain-Energy Distribution

To evaluate the contact strain-energy distribution comprehensively, an evaluation model is established. In the model, the uniformity of the contact strain-energy distribution is evaluated in three levels, by overall entropy, regional entropy, and local entropy. The difference between the three levels of entropy evaluation is the range of the strain energy. In the first level, the overall entropy is the overall evaluation of the strain-energy distribution of the entire mating surface. The entire mating surface includes the direct contact area, contact impact area (which does not have direct contact but is affected by deformations of the surrounding area), and non-impact area (which does not have direct contact and is not affected by deformations of the surrounding area). Although the evaluation of this level only roughly reveals the influence of the strain-energy distribution on the final assembly accuracy, when the results of the overall entropy show that the strain-energy distribution is good enough, it is not necessary to perform the following more detailed evaluations of the other levels. In the second level, the regional entropy is the evaluation of the strain-energy distribution of the direct contact area and the contact impact area. Similarly, when the results of the regional entropy show that the strain-energy distribution is good enough, it is no necessary to perform the last evaluation level. Otherwise, the local entropy should be calculated in the last evaluation level, which is the evaluation of the strain-energy distribution of the direct contact area and reflects the influence of the strain-energy distribution on the final assembly accuracy maximally. After performing the three levels of evaluation, a comprehensive evaluation index is obtained as follows.

$$H_M = \alpha \cdot H_{0s} + \beta \cdot H_{rs} + \gamma \cdot H_{cs} \tag{8}$$

where H_M is the weighted average entropy, and α, β, and γ are the weights. According to the contribution of each evaluation level in predicting the influence of the strain-energy distribution on the final assembly accuracy, the weights should be satisfied with $\alpha < \beta < \gamma$. In addition, the values of the weights should be considered in accordance with the processing technology, materials, and assembly parameters of the parts. H_{0s} is the overall entropy for evaluating the distribution of the contact strain energy of the PSL, which is the primary level of evaluation. If H_{0s} indicates that the distribution of the contact strain energy is uniform ($H_{0s} > 0.8$), the weights of α, β, and γ can be taken as $\alpha = 1$, $\beta = 0$, and $\gamma = 0$. On the contrary, if H_{0s} indicates that the distribution is nonuniform ($H_{0s} \leq 0.8$), a second level of evaluation needs to be carried out to further analyze the degree of nonuniformity. The regional entropy H_{rs} is calculated for the second level of evaluation to analyze the uniformity of the distribution of the contact strain energy within the contact and potential contact deformation regions. If $H_{rs} > 0.9$, the weights can be set as $\alpha = 0.2$–0.3, $\beta = 0.7$–0.8, and $\gamma = 0$. As the overall entropy is a basic evaluation of the distribution of the contact strain energy, the value of α is relatively small. As the regional entropy H_{rs} reflects the distribution of the contact strain energy in the contact and potential contact deformation regions, the value of β is referenced to the Young's modulus of the material. A material with a small elastic modulus takes a large value of β, and a material with a large elastic modulus takes a small value of β. If $H_{rs} \leq 0.9$, a third level of evaluation needs to be conducted to analyze the distribution of the contact strain energy on the direct contact area. After the calculation of the local entropy H_{cs}, the weights can be set as $\alpha = 0.15$–0.2 and $\beta = 0.2$–0.35. β depends on the material, for example, $\beta = 0.3$

for aluminum, and β = 0.25 for iron. As the local entropy H_{cs} reflects the state of the distribution of the contact strain energy directly, the value of γ is more than or equal to 0.5.

Figure 4 shows the specifics of the evaluation model for the distribution of contact strain energy.

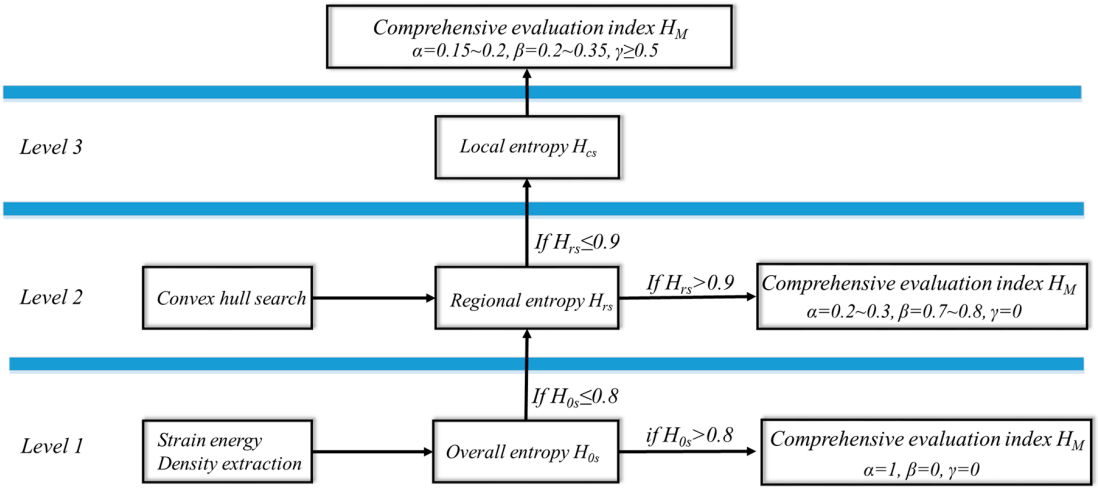

Figure 4. Evaluation model of distribution of contact strain energy.

3. Methodology

3.1. Primary Evaluation of Contact Strain-Energy Distribution

According to the entropy evaluation method, prior to the calculation of the overall entropy, the strain-energy density of the contact surfaces of the parts is first obtained.

3.1.1. Strain-Energy Density Extraction of the Contact Surfaces of the Parts in the Assembly

Because of the existence of form error, there are peaks and valleys on the PFE. Contact mainly occurs between the peaks and valleys. Only by obtaining the actual properties of the contact surfaces of the parts and developing the contact model with such parts, we can reflect the actual contact state in the assembly.

Figure 5 shows the process for evaluating the strain-energy density.

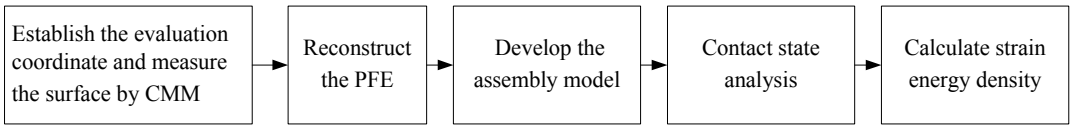

Figure 5. Process of strain-energy density extraction.

First, a series of measuring points characterizing the surface form error of the PFE are measured using a coordinate measuring machine (CMM). Then, the PFE is reconstructed based on the method of Bi-cubic B-spline surface interpolation using the point coordinate values measured by CMM [34] in order to develop a 3D solid model of the part. Thereafter, the assembly model is built by assembling an ideal part onto the part, and the PFE becomes the contact surface of the assembly. Finally, the assembly model is divided into elements by finite element simulation software. To ensure the accuracy of the extraction of the strain-energy density, the density of the element division grid must be greater than the density of the measurement grid, as shown in Figure 6. For precisely machined surfaces, the plane form error is very small (even less than 5 μm); to display the uneven height of surfaces, *Z* coordinate values of the PFE are magnified 100 times (shown in Figure 6). Hereafter, we always use this display method. A general milling part is taken as an example.

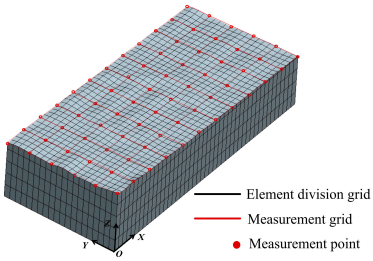

Figure 6. Schematic of the grid density.

In the following contact simulation analysis, an appropriate uniform pressure load, which will not generate plastic deformation, is applied on the top surface of the mating part. Then, the strain energy density can be calculated using the values of stress, strain, and volume for each element. Figure 7 shows the contact stress contour of the evaluation part (the ideal part of the top is not displayed).

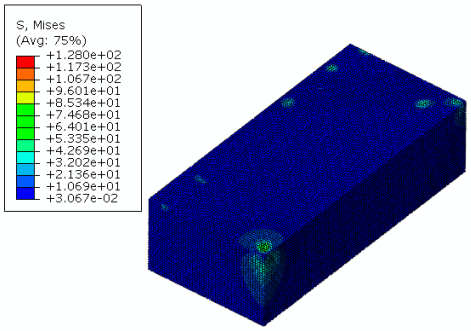

Figure 7. Contact stress contour.

3.1.2. The Overall Entropy Calculation

The contact strain-energy distribution of the PSL is primarily evaluated. The calculation method of the overall entropy evaluation is as follows:

The overall entropy, H_0, of the PSL is calculated using

$$H_0 = -\sum_{i=1}^{m} w_i' \log 2 w_i' \tag{9}$$

The corresponding maximum entropy can be expressed as

$$H_{0\max} = \log_2 m \tag{10}$$

The normalized overall entropy can be expressed as

$$H_{0s} = \frac{H_0}{H_{0\max}} \tag{11}$$

If H_{0s} is very close to 1, it indicates that the strain energy densities of the elements of the PFE are close to each other, which implies that the uniformity of the contact strain-energy distribution is sufficient. If H_{0s} indicates that the uniformity of the contact strain-energy distribution is insufficient, the following analysis should be conducted.

3.2. Regional Evaluation of Contact Strain-Energy Distribution

In the assembly process, the actual contact area between the parts is considerably smaller than the nominal contact area. When a part with PFE mates with another part with an ideal surface, it can be

seen as the contact between an ideal surface and a finite number of convex hulls on the PFE. Moreover, contact deformation, which causes the assembly error, mainly occurs in the convex hulls contacted in assembly. Therefore, convex hulls on the PFE, which are the contact and potential contact deformation regions, should be searched.

3.2.1. Convex Hull Search

To search all the convex hulls on the surface, we defined the CHI previously, and the location of the CHI needs to be determined first.

Cross planes, which pass through the convex hulls, are defined as a series of planes, parallel to the *X*-*O*-*Y* plane with the same size as that of the PFE. An appropriate initial position of the cross planes σ and the distance between the cross planes Δz are selected according to the Z coordinate values of the measuring points. The cross plane is named as the jth cross plane (j = 1, 2, 3 . . .) with respect to height, from highest to lowest. The height of the jth cross plane can be calculated as

$$h_j = z_{\max} - \sigma - (j-1)\Delta z \tag{12}$$

where $z_{\max}$ is the maximum value of z for the measuring points on the PFE. All the measuring points are projected on each cross plane beneath them. That is, if a measuring point is under the cross plane, which is $z_i < h_j$, it will have no projection on the cross plane. Thereafter, projection points on the CHI are divided into several clusters using the iterative self-organizing data-analysis technique algorithm (ISODATA) [35]. Each cluster consists of a convex hull.

The convex hulls composed by projected points on the 1st to 8th cross planes for the milling part surface mentioned previously with a size of 115 × 50 mm are shown below (Figure 8). σ and Δz take the values 0.01 and 0.001, respectively. The rectangles show the outline of the section cross-plane, and the circles show the convex hull clustered by the projected points.

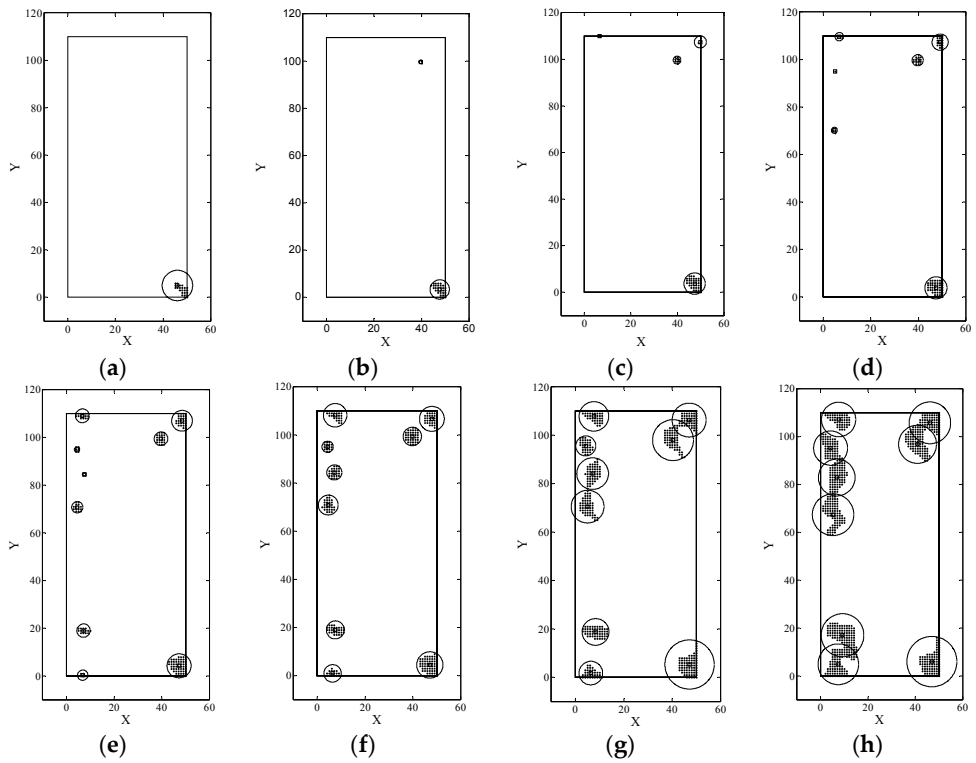

Figure 8. Clustering results of the projection points on each cross plane. (**a**) The 1st cross plane; (**b**) The 2nd cross plane; (**c**) The 3rd cross plane; (**d**) The 4th cross plane; (**e**) The 5th cross plane; (**f**) The 6th cross plane; (**g**) The 7th cross plane; (**h**) The 8th cross plane.

The area ratio of the convex hulls, the entire cross plane k, and the convex hull number p for each cross plane are calculated. With the decrease in the height of the cross plane, p and k change, as shown in Figure 9.

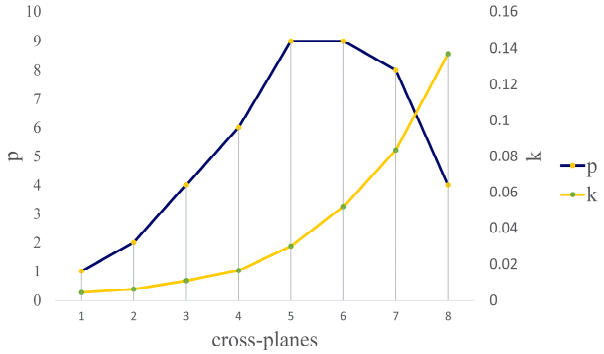

Figure 9. Area ratio and convex hull number for each cross plane.

The CHI should have relatively large values for p and k. Before the 4th cross plane, the convex hull number p is relatively small, which indicates that these cross planes pass through several high-convex hulls. With the height of the cross plane further decreasing, p and k increase accordingly. After the 6th cross plane, k still increases, but p decreases, which reveals that a convex hull fusion occurred. When the fusion occurred, the cross planes pass through the base layer of the part; hence, the points on these cross planes are composed of the base rather than the convex hulls. For the 5th and 6th cross planes, the 6th cross plane has the same p, but a larger value of k as compared to that of the 5th cross plane, which indicates that the 6th cross plane is closer to the bottom of the convex hulls. Overall, the 6th cross plane is determined as the CHI.

It should be noted that if the surface of the parts were an inclined plane or had a direct current (DC) component characteristic, the determination of the CHI would be affected by the DC component. To search the convex hull accurately for further evaluation, the DC component should first be removed from the measuring points.

3.2.2. Regional Entropy Calculation

The convex hulls have been searched, as observed in Section 3.2.1 (the milling part mentioned above). According to the position and size of the convex hulls shown in Figure 8f, the elements composing the convex hull at the contact surface (Figure 7) can be extracted.

Furthermore, H_r can be calculated using the strain energy densities of these elements.

$$H_r = -\sum_{i=1}^{m_c} w'_{ri} \log_2 w'_{ri} \tag{13}$$

where m_r is the number of elements composing the convex hulls, and w'_{ri} is the normalized strain-energy density of these elements.

The corresponding maximum entropy can be calculated as

$$H_{r\max} = \log_2 m_r \tag{14}$$

The normalized regional entropy can be calculated as

$$H_{rs} = \frac{H_r}{H_{r\max}} \tag{15}$$

If the distribution of the height and the location of the convex hulls are uniform, the convex hulls more equally bear the assembly force. Therefore, the strain energy distribution within the convex hulls is more uniform, without stress concentration and large contact deformation, and H_{rs} is larger. Otherwise, if the distribution of the height and location of the convex hulls are uneven, the assembly contact points could bear unequal assembly forces and produce unequal deformations, which will generate additional assembly errors and reduce the assembly accuracy. Therefore, as the uniformity of the contact strain-energy distribution within the region of the convex hulls increases, there would be better assembly accuracy.

3.3. Local Evaluation of Contact Strain-Energy Distribution

The assembly error produced in the process of assembly is more relevantly reflected by the strain-energy distribution of the direct-contact area. The local contact strain-energy distribution is evaluated to analyze the uniformity of the contact strain-energy distribution of the direct contact area in the assembly (the highlighted area in the contact-stress contour, as shown in Figure 7). The local entropy H_c is calculated using the strain energy densities of the direct contact elements in the assembly.

$$H_c = -\sum_{i=1}^{m_c} w'_{ci} \log_2 w'_{ci} \tag{16}$$

where m_c is the number of elements in the direct contact area, and w'_{ci} is the normalized strain-energy density of these elements.

The corresponding maximum entropy can be calculated using

$$H_{c\max} = \log_2 m_c \tag{17}$$

The normalized local entropy can be calculated using

$$H_{cs} = \frac{H_c}{H_{c\max}} \tag{18}$$

If the local contact strain-energy distribution is more uniform, it indicates that there are no evident stress concentration and uneven deformations, and H_{cs} will be larger. As uneven deformation produces additional assembly error and reduces the assembly accuracy, few uneven deformations and less tress concentration are advantageous to obtain better assembly accuracy.

4. Experimental Verification

4.1. Experimental Setup

To verify the effectiveness of the evaluation method, five groups of assemblies are designed. Figure 10 shows the assembly of two components, which are both axisymmetric. The surface M_A of part A contacts with the surface M_B of part B. The two mating surfaces are identical and plane circular, with a diameter of 62 mm. The two components are fastened together by four clamping bolts with preloads of F_1, F_2, F_3, and F_4. The material of part A is carbon steel treated with quenching and tempering processes. The flatness of the surface M_A is designed to be 5 μm. The material of part B is 7075 aluminum.

The assembly accuracy requirement is the coaxiality between the cylindrical surface A of part A and the cylindrical surface B of part B; the coaxiality is denoted by Ω, which is used as the verification index to characterize the assembly accuracy. We first installed the two pins for a rough positioning of the parts. We then moved away the pins. To avoid the positioning error, after the pins are moved away, we narrowly adjusted the position of the two parts in such a way that the coaxiality of the surfaces A and B is within 3 μm. Thereafter, we used the torque wrench (Motive-ZDP20, ± T·0.3%) to apply equivalent preloads (0.6 N·m) for all the four bolts. Thereafter, we measured the value of Ω. Hence,

the coaxiality between the surfaces A and B is only affected by the form errors of the mating surfaces and the contact deformations.

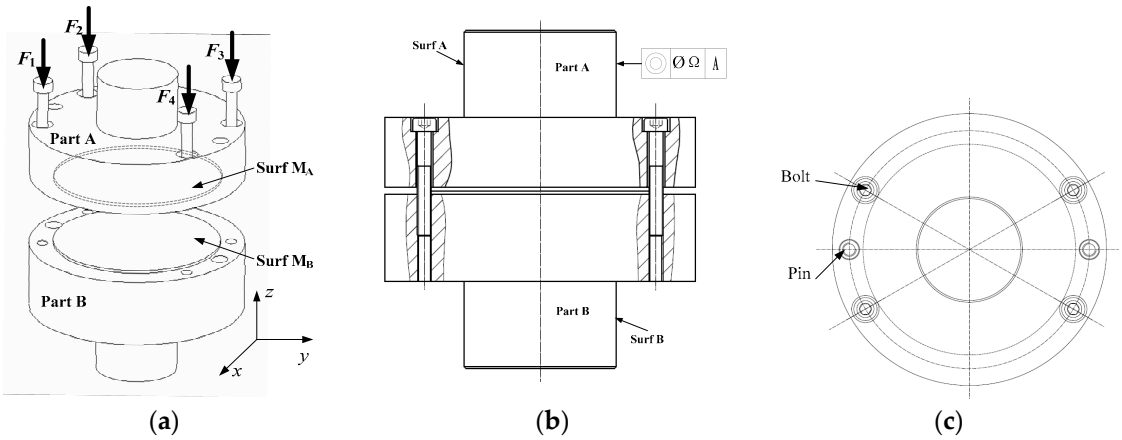

Figure 10. Assembly schematic of two components. (**a**) Exploded view; (**b**) Main view; (**c**) Top view.

4.2. Comparison between Assembly Accuracy Prediction and Experimental Results

Coordinate measurements of mating surfaces for part B are carried out by CMM"PMM12106G", whose measurement uncertainty is $(0.6 \pm L/600)$ μm. We only focused on the Z coordinate values of all the measurement points, and the total standard deviations of the measurement data are between 10 μm to 20 μm; therefore, the measurement uncertainty can be ignored [36]. The actual flatness errors of surface M_B of part B for each group are measured, as presented shown in Table 1. Thereafter, the 3D solid models of part B are developed, as displayed in Figure 11. In addition, we also measured the flatness and roughness of surface M_A of part A. The flatness is around 5 μm and the roughness is around Ra = 0.4 μm.

Table 1. Actual flatness errors of surface $M_B$of part B for each group.

	M_B 1	M_B 2	M_B 3	M_B 4	M_B 5
Flatness errors/μ	62	62	63.5	62	62

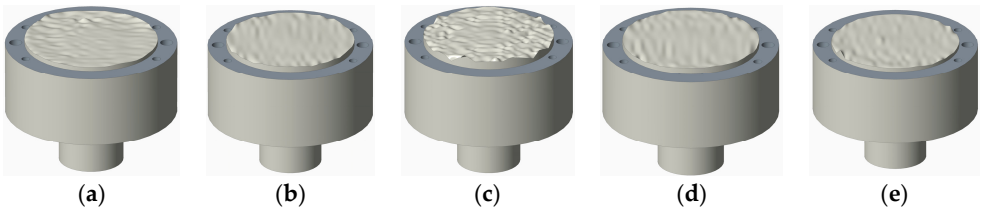

Figure 11. 3D solid model of parts B (Z values magnified 100×). (**a**) B1; (**b**) B2; (**c**) B3; (**d**) B4; (**e**) B5.

To obtain the strain energy, the contact state is analyzed by FEM. The simulation parameters and boundary conditions are shown in Table 2.

Because the flatness of the contact surface of part A is relatively good, it is regarded as an ideal surface for FEM simulation. The preload value can be calculated by the following equation,

$$T = \lambda \cdot F \cdot d \tag{19}$$

where T is torque (T = 0.6 N·m); F is the preload of bolts (N); λ is the torque coefficient (here we take λ = 0.2) [37]; and d is the bolt diameter (d = 4 mm). The simulation model and stress contours are shown in Figure 12.

Table 2. Simulation parameters and boundary conditions.

Terms	Parameters	Values
Software setting	Software	ABAQUS
	Type of contact	Surface-to-surface
	Type of simulation	Explicit
Elements	Type of element	C3D8I
	Formulation of the element	Linear
Material	Carbon steel (part *A*)	210 GPa (Young's modulus) 0.3 (Poisson's ratio)
	7075 Aluminum (part *B*)	70 GPa (Young's modulus) 0.32 (Poisson's ratio)
Boundary conditions	Preload of bolts	$F_1 = F_2 = F_3 = F_4 = 750$ N

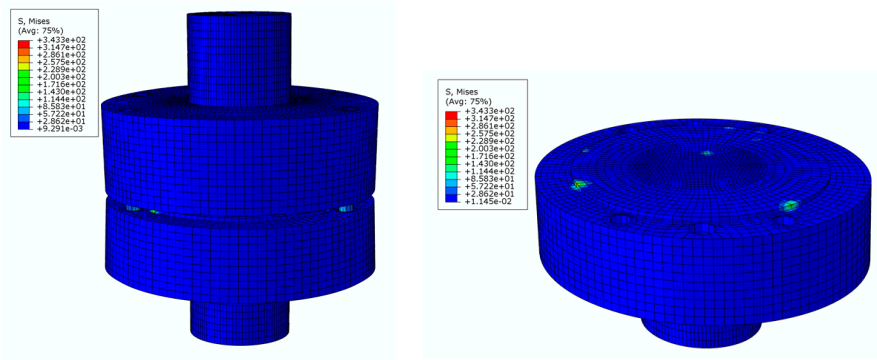

Figure 12. Simulation model and stress contours. (**a**) Stress contour of the entire model (magnified 300×); (**b**) Stress contour of part *B*.

Thereafter, the strain-energy density is extracted. Figure 13 shows the assembly-contact stress contours of the PSL. The convex-hull searching is carried out. Figure 14 shows the results.

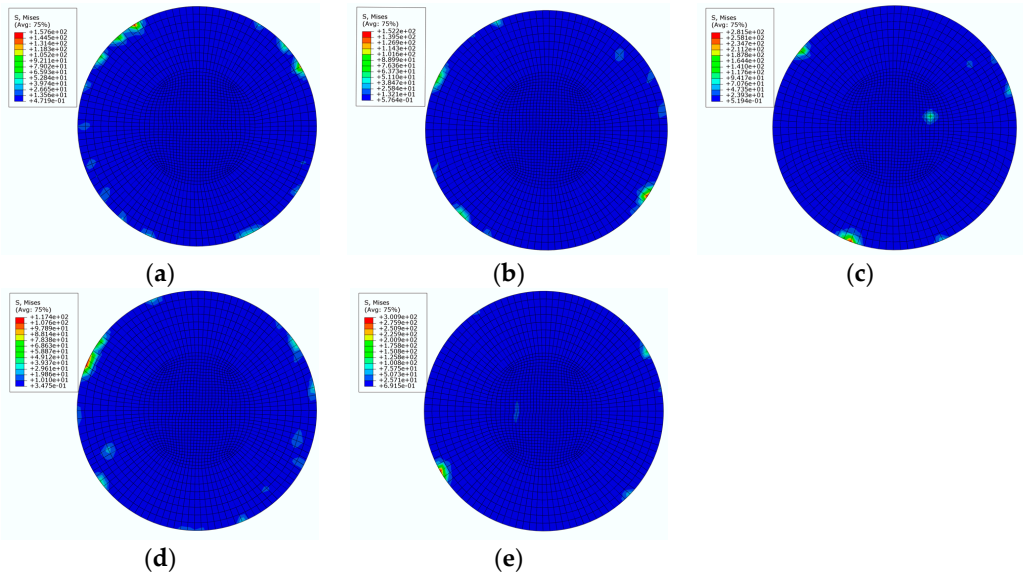

Figure 13. Contact stress contour for the PSLs of each part *B*. (**a**) Group 1; (**b**) Group 2; (**c**) Group 3; (**d**) Group 4; (**e**) Group 5.

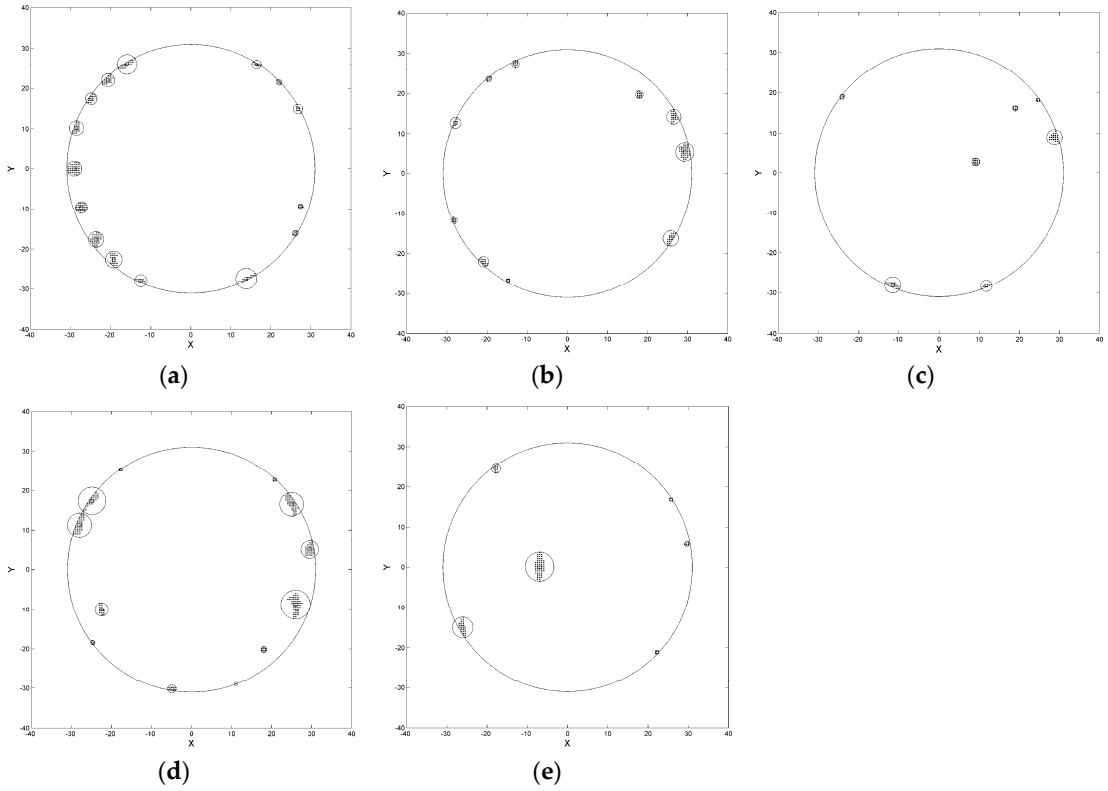

Figure 14. Convex-hull searching results. (**a**) Group 1; (**b**) Group 2; (**c**) Group 3; (**d**) Group 4; (**e**) Group 5.

Thereafter, we calculate the overall entropy, the regional entropy, and the local entropy for each group of assemblies. In addition, according to the processing technology, material, and assembly parameters of the parts, the values of the weights are set as $\alpha = 0.2$, $\beta = 0.3$, and $\gamma = 0.5$. Then, the comprehensive entropy evaluation index can be expressed as follows:

$$H_M = 0.2 \cdot H_{0s} + 0.3 \cdot H_{rs} + 0.5 H_{cs} \tag{20}$$

Ultimately, the coaxiality between the cylindrical surfaces A and B is measured using the Mitutoyo Round Test RA-1500, and the measurement uncertainty of which is ± 0.02 μm (shown in Figure 15), the measurement results of which are shown in Figure 16. Table 3 lists the results of the evaluation of entropies and experiments.

Figure 15. Experimental setup.

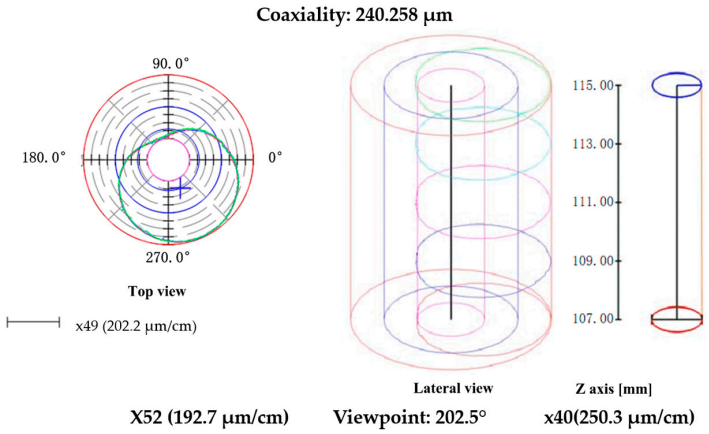

Figure 16. Measurement coaxiality results of Group 3.

Table 3. Results of evaluation of entropies and experiments.

	Group 1	Group 2	Group 3	Group 4	Group 5
H_{0s}	0.5660	0.6654	0.5531	0.5630	0.5046
H_{rs}	0.7957	0.7647	0.7380	0.7811	0.7543
H_{cs}	0.8757	0.8659	0.7670	0.7701	0.7070
H_M	0.78976	0.79544	0.71552	0.73198	0.68071
$I = \Omega/\mu m$	141.663	102.39	240.258	233.853	402.248

According to the results obtained by the evaluation model, the results of the comprehensive entropy evaluation of the five groups of assemblies show that the comprehensive evaluation index H_M of Group 2 is the largest; it is the smallest for Group 5. It indicates that when these groups of parts are assembled, Group 2 will gain the best assembly accuracy, and Group 5 will obtain the worst assembly accuracy. According to the experimental results of the verification index Ω, which is the characterization of the assembly accuracy, it precisely confirmed the prediction; the coaxiality of Group 2 is the smallest, and the coaxiality of Group 5 is the largest. In addition to the coaxialities of the experimental results, it can also make a qualitative interpretation of assembly accuracy from the contact stress contour (Figure 13) and the searching results of the convex hulls of the mating parts (Figure 14). Figure 13 reveals that stress concentrations occur in Group 5, and the convex hull position distribution of Group 5 is not uniform. Moreover, the stress concentration and non-uniformity of the convex hull position distribution will cause unsymmetrical and uneven assembly-contact deformations, which will significantly reduce the assembly accuracy. In contrast, Group 2 does not show significant stress concentration, and its convex hull distribution is relatively uniform. Therefore, Group 2 does not produce large assembly errors and obtains good assembly accuracy. In summary, the above results verify that the prediction method of assembly accuracy proposed in this paper is reliable and effective.

It should be noted that, if we take the values of weights as $\alpha = 0.15$, $\beta = 0.3$, and $\gamma = 0.55$ within their range of values, the prediction results are still in agreement with the experiment results. In addition, it can be seen from Tables 1 and 3 that the surface flatness cannot be used to predict the assembly accuracy, because the flatness of the five groups of parts is almost the same, but their assembly accuracy is very different. Therefore, the evaluation method for predicting the assembly accuracy proposed in this paper is reasonable and effective.

5. Conclusions

1. This paper has proposed an entropy-based method to evaluate the contact strain-energy distribution for predicting assembly accuracy. The strain energy is used to characterize the effects of the combination of form errors and contact deformation on the formation of assembly errors. In addition, entropy is employed to evaluate the distribution uniformity of the strain

energy. An evaluation model is built. The primary evaluation is first carried out, and regional and local entropy analyses are further implemented when the primary evaluation index is not satisfied. Finally, based on these calculation and analyses, a comprehensive evaluation index is obtained.

2. The form error of the real surfaces of the assembly parts and the contact deformations are considered. The 3D, solid model is developed. Moreover, the convex hull interface is defined, and all the convex hulls on the surface are searched. The FEM is used to analyze the assembly contact state subjected to the assembly forces. Ultimately, the coaxiality between the surfaces of the two parts with assembly accuracy requirements is assigned as the verification index for characterizing the assembly accuracy.
3. Through the comparison between the predicted results of the comprehensive evaluation index and the verification index obtained by the experiments, it is shown that the evaluation method of the contact strain-energy distribution for predicting the assembly accuracy proposed in this study is reliable and effective.

Acknowledgments: We would like to acknowledge the support of the National Natural Science Foundation of the People's Republic of China (No. 51375054 and U1537215).

Author Contributions: Yan Fang, Xin Jin and Zhijing Zhang conceived and designed the experiments; Yan Fang performed the experiments; Chencan Huang performed the finite element simulation analysis; Yan Fang and Chencan Huang analyzed the data; Xin Jin and Zhijing Zhang contributed materials and measuring instruments; Yan Fang wrote the paper. All authors have read and approved the final manuscript.

Conflicts of Interest: The authors declare no conflict of interest.

References

1. Liu, C.H. Tolerance Redistributing of the Reassembly Dimensional Chain on Measure of Uncertainty. *Entropy* **2016**, *18*, 348. [CrossRef]
2. Sieber, I.; Martin, T.; Gengenbach, U. Robust Design of an Optical Micromachine for an Ophthalmic Application. *Micromachines* **2016**, *7*, 85. [CrossRef]
3. Payne, J.R.; Fitzgerald Jerry Waterland, A., III. Variables Affecting the Assembly Bolt Stress Developed During Manual Tightening. In Proceedings of the ASME 2011 Pressure Vessels and Piping Conference, Baltimore, MD, USA, 17–21 July 2011; pp. 209–214.
4. Liu, W.; Li, L.; Kochhar, A.K. A method for assessing geometrical errors in layered manufacturing. Part 1: Error interaction and transfer mechanisms. *Int. J. Adv. Manuf. Technol.* **1998**, *14*, 637–643. [CrossRef]
5. Mansuy, M.; Giordano, M.; Hernandez, P. A Generic Method for the Worst Case and Statistical Tridimensional Tolerancing Analysis. *Procedia CIRP* **2013**, *10*, 276–282. [CrossRef]
6. Chase, K.W.; Parkinson, A.R. A survey of research in the application of tolerance analysis to the design of mechanical assemblies. *Res. Eng. Des.* **1991**, *3*, 23–37. [CrossRef]
7. Chase, K.W.; Gao, J.; Magleby, S.P.; Sorensen, C.D. Including geometric feature variations in tolerance analysis of mechanical assemblies. *IIE Trans.* **1996**, *28*, 795–808. [CrossRef]
8. Chase, K.W.; Magleby, S.P.; Gao, J. Tolerance analysis of two-and three-dimensional mechanical assemblies with small kinematic adjustments. In *Advance Tolerancing Techniques*; Wiley Interscience: New York, NY, USA, 1997; Volume 30, pp. 367–377.
9. Pierce, R.S.; Rosen, D. A method for integrating form errors into geometric tolerance analysis. *J. Mech. Des.* **2008**, *130*, 011002. [CrossRef]
10. Samper, S.; Adragna, P.A.; Favreliere, H.; Pillet, M. Modeling of 2D and 3D assemblies taking into account form errors of plane surfaces. *J. Comput. Inf. Sci. Eng.* **2009**, *9*, 041005. [CrossRef]
11. Grandjean, J.; Ledoux, Y.; Samper, S.; Favrelière, H. Form Errors Impact in a Rotating Plane Surface Assembly. *Procedia CIRP* **2013**, *10*, 178–185. [CrossRef]
12. Zuo, F.H.; Jin, X.; Zhang, Z.J.; Zhang, T.Y. Modeling method for assembly variation propagation taking account of form error. *Chin. J. Mech. Eng.* **2013**, *26*, 641–650. [CrossRef]
13. Armillotta, A. Tolerance Analysis Considering form Errors in Planar Datum Features. *Procedia CIRP* **2016**, *43*, 64–69. [CrossRef]

14. Samper, S.; Giordano, M. Taking into account elastic displacements in 3D tolerancing: Models and application. *J. Mater. Process. Technol.* **1998**, *78*, 156–162. [CrossRef]
15. Liu, S.C.; Hu, S.J. Variation simulation for deformable sheet metal assemblies using finite element methods. *J. Manuf. Sci. Eng.* **1997**, *119*, 368–374. [CrossRef]
16. Liu, J.Y.; Qiao, L.H. Calculation method for assembly error with consideration of part deformation. *Comput. Integr. Manuf. Syst.* **2015**, *21*, 94–100.
17. Liu, T.; Cao, Y.L.; Wang, J.; Yang, J.X. Assembly Error Calculation with Consideration of Part Deformation. *Procedia CIRP* **2016**, *43*, 58–63.
18. Zhou, C.Y. *Solid Mechanics in Materials*; Science Press: Beijing, China, 2005. (In Chinese)
19. Fazlollahtabar, H.; Olya, M.H. A cross-entropy heuristic statistical modeling for determining total stochastic material handling time. *Int. J. Adv. Manuf. Technol.* **2013**, *67*, 1631–1641. [CrossRef]
20. Lv, S.P.; Qiao, L.H. A cross-entropy-based approach for the optimization of flexible process planning. *Int. J. Adv. Manuf. Technol.* **2013**, *68*, 2099–2110. [CrossRef]
21. Zhang, Z.F. Manufacturing complexity and its measurement based on entropy models. *Int. J. Adv. Manuf. Technol.* **2012**, *62*, 867–873. [CrossRef]
22. Ahmed, S.S.; Messali, Z.; Ouahabi, A.; Trepout, S.; Messaoudi, C.; Marco, S. Nonparametric Denoising Methods Based on Contourlet Transform with Sharp Frequency Localization: Application to Low Exposure Time Electron Microscopy Images. *Entropy* **2015**, *17*, 3461–3478. [CrossRef]
23. Eguiraun, H.; López-de-Ipiña, K.; Martinez, I. Application of Entropy and Fractal Dimension Analyses to the Pattern Recognition of Contaminated Fish Responses in Aquaculture. *Entropy* **2014**, *16*, 6133–6151. [CrossRef]
24. Chakraborty, S.; Saha, S.; Corda, C. Hawking-Like Radiation from the Trapping Horizon of both Homogeneous and Inhomogeneous Spherically Symmetric Spacetime Model of the Universe. *Entropy* **2016**, *18*, 287. [CrossRef]
25. Frank, S.A. Common Probability Patterns Arise from Simple Invariances. *Entropy* **2016**, *18*, 192. [CrossRef]
26. Pollard, B.S. Open Markov Processes: A Compositional Perspective on Non-Equilibrium Steady States in Biology. *Entropy* **2016**, *18*, 140. [CrossRef]
27. Qi, F.; Li, C.; Wang, S.; Zhang, H.; Wang, J.; Lu, G. Contact-Free Detection of Obstructive Sleep Apnea Based on Wavelet Information Entropy Spectrum Using Bio-Radar. *Entropy* **2016**, *18*, 306. [CrossRef]
28. Shannon, C.E. A Mathematical Theory of Communication. *Bell Syst. Tech. J.* **1948**, *27*, 379–423. [CrossRef]
29. Chen, G.L.; Zhang, W.M. Angular Spectral Density and Information Entropy for Eddy Current Distribution. *Entropy* **2016**, *18*, 392. [CrossRef]
30. Xiao, J.; He, Z.Y. A Concept Lattice for Semantic Integration of Geo-Ontologies Based on Weight of Inclusion Degree Importance and Information Entropy. *Entropy* **2016**, *18*, 399. [CrossRef]
31. Özkan, K. Application of Information Theory for an Entropic Gradient of Ecological Sites. *Entropy* **2016**, *18*, 340. [CrossRef]
32. Robinson, D.W. Entropy and Uncertainty. *Entropy* **2008**, *10*, 493–506. [CrossRef]
33. Melia, U.; Claria, F.; Vallverdu, M.; Caminal, P. Measuring Instantaneous and Spectral Information Entropies by Shannon Entropy of Choi-Williams Distribution in the Context of Electroencephalography. *Entropy* **2014**, *16*, 2530–2548. [CrossRef]
34. Zhang, Z.Q.; Jin, X.; Zhang, Z.J. Study on modeling method of the precision machined surface geometry form error based on Bi-cubic B-spline. In Proceedings of the International Conference on Power Electronics and Energy Engineering (PEEE 2015), Hong Kong, China, 19–20 April 2015.
35. Ball, G.H., II; Hall, D.J. ISODATA, an iterative method of multivariate analysis and pattern classification. *Behav. Sci.* **1967**, *12*, 153–155. [CrossRef] [PubMed]
36. Fei, Y.T. *Error Theory and Data Processing*; Mechanical Industry Press: Beijing, China, 2008; Volume 1, pp. 95–145. (In Chinese)
37. Xu, H. *Machine Design Handbook*; China Machine Press: Beijing, China, 1991; Volume 3, pp. 44–45. (In Chinese)